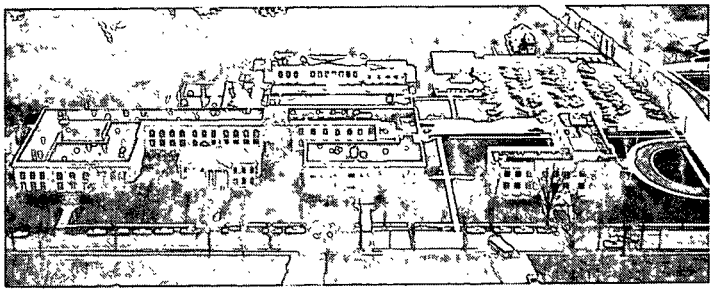

THE INSTITUTE OF PAPER CHEMISTRY, APPLETON, WISCONSIN

IPC TECHNICAL PAPER SERIES

NUMBER 296

SIMULATION OF THE PERFORMANCE CHARACTERISTICS OF A TMP MILL

GARY L. JONES

JULY, 1988

Simulation of the Performance Characteristics of a TMP Mill

Gary L. Jones

This manuscript is based on results obtained in IPC research and is to be presented at the 1988 Process Simulation Symposium of the Canadian Pulp and Paper Association in Quebec City, Quebec on Sept. 27-28, 1988

SIMULATION OF THE PERFORMANCE CHARACTERISTICS OF A TMP MILL

GARY L. JONES
ENGINEERING DIVISION

THE INSTITUTE OF PAPER CHEMISTRY
APPLETON, WISCONSIN 54912

ABSTRACT

Fiber and handsheet properties throughout a TMP mill operation have been successfully simulated by means of the MAPPS performance attribute system. Bauer-McNett fiber length classifications, shives, freeness and a variety of tensile and optical properties from eight widely-separated streams in the process compare favorably with measured values. The models are described qualitatively. Expansion of the system to predict property development during chemical pulping and papermaking is discussed.

INTRODUCTION

Mechanical pulping processes represent a growing segment of pulp production. High yield pulps are now commonly blended with chemical pulps to produce a variety of paper grades. The operations involved in making mechanical pulps such as refining, screening, cleaning and bleaching all influence the final properties of the sheet. It is now possible to simulate some of the effects of each operation on the development of sheet properties through the performance attribute (PAT) system available in MAPPS [1].

Performance attributes are variables which are fundamental to the properties and end-use characteristics of the individual fibers and fiber network. The PAT system consists of PAT models which initialize and modify PAT's and PROP models which compute pulp and sheet properties (PROP's). Some aspects and applications of the PAT system have been described previously [2,3].

The PAT system was developed from models and experimental data from a variety of sources [4,5,6,7,8,9] and assembled in novel and unique ways. Performance attributes of interest to the simulation of high yield pulping are ODW yield, average fiber cell-wall thickness, weight-average fiber length, standard deviation of fiber length distribution, number-average fiber width and standard deviation, Canadian Standard Freeness, CSF, K-factor, and absorption coefficient.

MAPPS is a sequential modular simulator consisting of modules representing operations connected by streams representing flows of material, energy or information. Each physical stream has an associated PAT stream containing the performance attribute values for the material in that stream.

OBJECTIVE

The purposes of this work were to validate the PAT system for simulation of high yield pulping and to better understand the factors contributing to property development. The validation was made possible through a comparison of the simulation results with data from a TMP mill producing unbleached pulp.

DISCUSSION

The TMP process of interest is represented schematically as a MAPPS flowsheet in Figure 1. Three types of MAPPS process modules are used to represent the actual process units: refiner modules represented by HYRFN1, stock separation modules represented by HYFRAC and stock mixing, STOMIX.

The flowsheet is converged by testing tear stream 53 with a convergence module not shown. The convergence loop is set up to return to stock tank, module 24. Although there are a number of tear streams, the material balances are satisfied by testing only one tear stream. Both direct substitution and accelerated convergence techniques (Wegstein) were used.

HYRFN1 blocks 1,2 and 19 simulate the chip refiner, secondary refiner and reject refiner, respectively. Each refiner has two entering streams, a pulp stream and a net specific power stream. Leaving each refiner are three streams representing refined pulp, heat loss and a dirty steam. For the chip refiner these streams are 6,101,2,102,103, respectively.

HYFRAC modules simulate screening, cleaning and thickening operations. HYFRAC modules 5, 33 and 34 represent primary screen, secondary screen and sidehill screen. The screen is indicated by '(1)' under the name HYFRAC. Modules with '(2)' under the name [e.g., 8,10,11, etc.] represent centricleaners. Thickeners with complete fines retention are designated by '(3)', while thickeners with some fines loss to the rejects are designated by '(4)'. The accept streams are indicated by "acc" and the rejects by "rej".

Entering the process are chip and water, streams 1 and 4. Streams 32, 31, and 47 represent the thickened stock, sewer rejects and

excess white water leaving the process. White water is passed throughout the flowsheet to provide a relatively closed system. Essentially all streams are composed of the following: fibers, shives, fines, dissolved solids, suspended solids, and water.

Fibers consist of five Bauer-McNett screen classifications. Fiber 5 > 14, 28 < Fiber 4 < 14, 48 < Fiber 3 < 28, 100 < Fiber 2 < 48, 200 < Fiber 1 < 100 mesh. Fines are less than 200 mesh. All fibers and fines are defined to pass through a 0.00015 m Sommerville slot. Shives are defined to be held on a 0.00015 m Sommerville slot. There are three shive categories: 0.00015 m < Shive 1 < 0.00075 m, 0.00075 m < Shive 2 < 0.00125 m, and Shive 3 > 0.0015 m, respectively. All shives are assumed to occupy the entire length range (i.e., shives are independent of length).

The chip refiner converts chips with average dimensions (typically 0.025 x 0.005 m) into mixtures of fibers, fines and shives having independent distributions of length and width. Secondary and reject refiners convert the inlet pulp stream with one set of distributions into an outlet pulp stream with a different set of distributions. The refiners also generate surface area (hydrodynamic specific surface) and alter the CSF. These in turn influence sheet properties.

The fiber residence time within the refiner is an exponential function of net specific power to the refiner. The fiber residence time and other parameters determine the change in the average and standard deviation of the fiber length and width distributions. The distributions are then manipulated to determine the measured components such as the fibers, fines and shives.

Many refiner pulps have a log-normal fiber length distribution [10]. However, in a number of situations, the distribution deviates significantly from log-normality. In effect, a portion of the distribution between 14 and 48 mesh and that between 200 and 48 mesh are reversed. The causes of the differences are not known. HYRFN1 allows for either type of distribution. The modified log-normal distribution best described that observed from the secondary refiner in the TMP process. Despite the considerable effect of processing conditions, this distribution persisted throughout the process.

Hydrodynamic specific surface area varies with fiber length and is a function of refiner power, refining consistency and entering surface area. The influence of refining on surface area

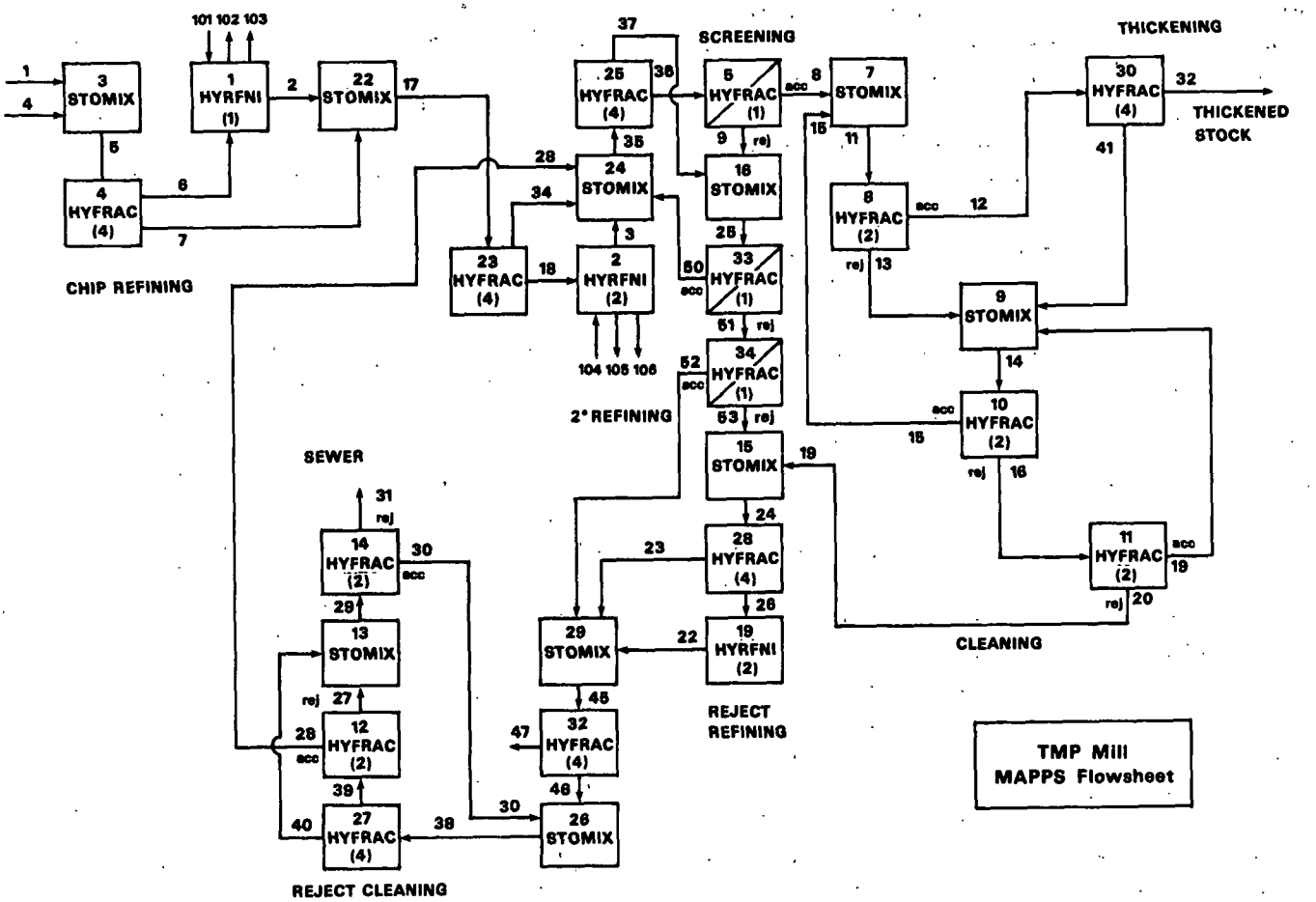

Fig. 1. MAPPS TMP process flowsheet.

development is lumped into a single factor, the K-factor, which is passed throughout the flowsheet in the performance attribute stream. The surface area can be determined from the K-factor and the fiber length distribution. The K-factor is only modified in the refiners and is not affected by fiber separations or stock mixing.

CSF is assumed to be a function of hydrodynamic specific surface and is assumed to be interchangeable with it. The relationship between CSF and specific surface is also dependent on yield. Bonded area is a function of yield or lignin distribution within the fibers and hydrodynamic specific surface. Bonded area is increased by wet pressing and is reduced by reslurrying. Sheet density is then determined by bonded area, unbonded density and maximum density. The latter two variables are functions of yield, CSF, and cell-wall thickness.

Sheet tensile and optical properties are related to sheet density, fiber modulus, zero span tensile, the contents of shives, long fibers and fines, absorption coefficient and other performance attributes. These are the PROP models referred to above. Relative bonded area is assumed to be a function of sheet density. Property models are based on a variety of sources [11,12,13] and are currently undergoing evaluation and testing.

Throughout the PAT system, the PAT distribution statistics (mean and standard deviation of length and width) are used to compute the discrete distributions of length and width. A matrix is constructed from these discrete distributions representing the weight fraction of fibers within each of the 100 individual length-width categories. Operations are performed on this "correlation" matrix to effect mixing, separation and refining.

The HYFRAC modules separate fiber particles based on their length and width values within the correlation matrix. The screen separation efficiency function operates on the matrix of the inlet stream to produce an accept stream and a reject stream matrix. These are then used to construct the accept and reject fiber components.

Screens tend to separate on the basis of fiber length, while hydrocyclone cleaners separate on aspect ratio (L/W). The relationships between length distribution and surface area results in an indirect separation based on surface area. The separation process then influences the K-factor, CSF, fiber length and width distributions of the accept and reject streams. Differences in these PAT's then bring about variations in properties of the outlet streams.

The mixer modules (STOMIX) combine one or more stock streams. Mixing of streams produces a mixture of PAT's. The mixture PAT's then determine mixture properties. Some of the mixing rules are based on conservation of hydrodynamic specific surface area. Other PAT's are mixed based on a weighted-average of the inlet streams.

Input data include the following: refiner specific power for the three refiners, overall mass (or volumetric) flow splits for each of the screens or hydrocyclones, outlet consistency for each of the thickeners and streams containing chips, water, dissolved and suspended solids. Other input data include fiber cell-wall thickness, yield and wet pressing pressure. These were assumed to be 1.8 microns and 100% based on ODW and 414 kPa, respectively.

Some data needed as input to MAPPS were not available and had to be assumed. Other data were provided which were not required as input but were predicted by the simulation. Only rough estimates of gross refiner power were provided. The net refiner specific power values actually used by the refiner model were chosen by experience. In particular, the net power into the secondary refiner was adjusted to give a reasonable fit to the measured fiber distribution and CSF in stream 3.

Shive data was in the form of a 4-cut which represented a 0.0001 m slot width, while the simulation generated a shive cut based on a 0.00015 m slotted Sommerville screen.

One function of the screening and cleaning system is to remove dirt and debris. Although no data were available for this aspect of the process, the physical property data indicated indirectly that the effect of dirt was minor.

The following process data were provided: consistencies throughout the flowsheet, general levels of fiber splits on the screens and cleaners, fiber flows through the reject system and fraction fibers lost to sewer (stream 31). Processing conditions used in or computed by MAPPS are summarized in Tables I through III. Property data are summarized later. Numbers in parentheses indicate stream or module numbers in Figure 1.

Duplicate fiber and shive classification and handsheet property data were provided at eight locations in the process. Because the replications were quite close, only one set of data values is presented.

Table I. Simulated Processing Conditions.

	Net Specific Power Kj/tonne	Inlet Consistency %
Chip Refiner (1)	2.7	35
Secondary Refiner (2)	3.55	25
Reject Refiner (19)	2.7	28

	Specified Total Flow Split %	Predicted Fiber Yield %	Predicted Shive Removal Efficiency %
Reject Rates			
Primary Screen (5)	10	79	44
Secondary Screen (33)	33	47	63
Sidehill (34)	25	50	58
Cleaners			
Primary (8)	10	82	35
Secondary (10)	30	63	50
Tertiary (11)	10	81	35
Reject (12)	10	62	38
Reject (14)	10	62	38

Splits are reject mass flow/inlet flow.

Table II. Process Flows BD Fiber (kg/s).

	Data	Simulation
Chips Entering (1)	1.62	1.62
Total Production from Thickener (32)	1.58	1.54
Reject Refiner Throughput (26)	0.26	0.22
Sewer Losses (31)	0.03-0.04	0.07

Table III. Screen and Cleaner Consistencies (%).

	Data	Simulation
Primary screen (5)	(Estimated)	
Inlet (36)	1.2	1
Accepts (8)	1.0	0.9
Rejects (9)	1.3	2.0
Secondary Screen (33)		
Inlet (25)	1.3	1.1
Accepts (50)	0.9	0.8
Rejects (51)	1.6	1.7
Sidehill Screen (34)		
Inlet (51)	1.6	1.7
Accepts (52)	0.2	1.0
Rejects (53)	2.5	3.1
Rejects Press (28)		
Inlet (24)	2.5	2.5
Accepts (23)	0.2	0
Rejects (26)	28.0	28
Primary Cleaner (8)		
Inlet (11)	1.0	1.3
Accepts (12)	0.4	0.6
Primary Reject Cleaner (12)		
Inlet (39)	--	2.0
Accepts (28)	0.35	1.4
Thickener (30)		
Accepts (32)	4.0	4.0
White Water (41)	0.1	0

The correspondence between the eight locations (position numbers 1 through 8) and the stream numbers in the flowsheet are shown in Table IV. Fiber classification and handsheet property data are summarized in Figures 2 through 11.

Handsheet properties are computed from one of two classes of models. The first class consists of simple correlations of properties in terms of the fractions of long fibers shives and fines and CSF [4].

Table IV. Correspondence Between Sampling Position and MAPPS Flowsheet Stream Numbers.

Position		MAPPS Stream Number Figure 1
1	Secondary Refiner Discharge	3
2	Primary Screen Feed	36
3	Primary Screen Accepts	8
4	Primary Screen Rejects	9
5	Secondary Screen Accepts	50
6	Reject Refiner Discharge	22
7	Primary Reject Cleaner Accepts	28
8	Thickener Discharge	32

Tear and scattering coefficient which depend on fiber length distribution, the number of particles and fines content are predicted from these correlative models. Other performance factors computed from these models are wet web strength, drainage time and opacity. Wet web strength is strongly dependent on shive content while drainage time and opacity depend strongly on fines content.

Models in the second class were developed from chemical pulping data and are more fundamental in nature. These models can be extrapolated, at least in the present situation, to the TMP yield range. They require the fiber cell-wall thickness, wet pressing pressure, CSF, and yield. Handsheet properties calculated by these models are TAPPI density, elastic modulus, breaking length, burst factor, stretch, rupture energy and Gurley porosity.

Scattering coefficient and tear are also predicted for pulps in the typical chemical pulp yield range of 48 to 60%. However, these property models in their current forms do not extrapolate to high yields. In the future, anisotropy ratios, formation, compressive strength, Z-D properties, absorption coefficient and brightness will be determined by the system.

Figures 2 and 3 show the close correspondence between the measured and simulated variations at positions 1 through 8. The fines most often are the largest single fiber fraction. The longest fiber fractions together represent from 35 to 60% of the pulp. Fines decrease and long fibers increase in primary screen rejects and secondary screen accepts. The fiber distribution in the thickened stock is remarkably similar to the secondary refiner discharge, however.

Figures 4 and 5 provide further detailed comparisons of fiber morphology in each stream. Shives shown in Figure 4 tend to be more con-

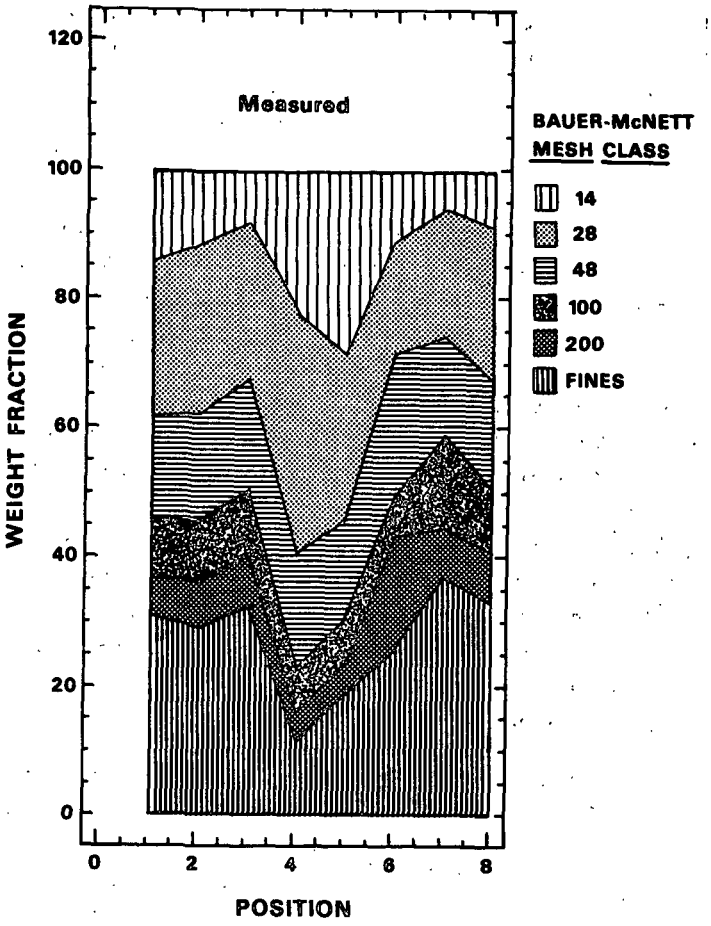

Fig. 2. Measured fiber length distributions.

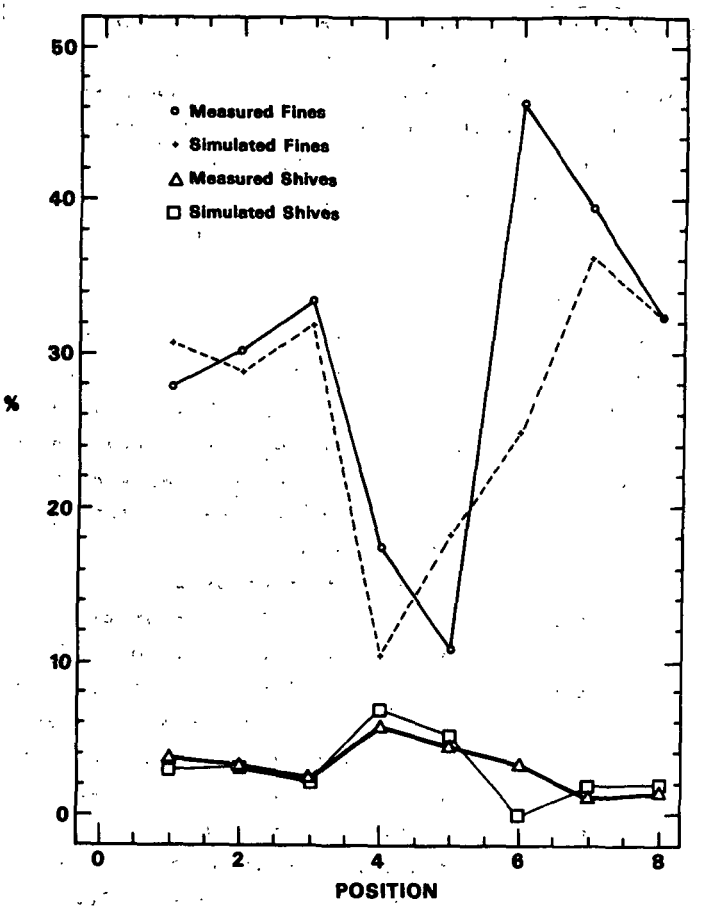

Fig. 4. Fines and shives vs. position.

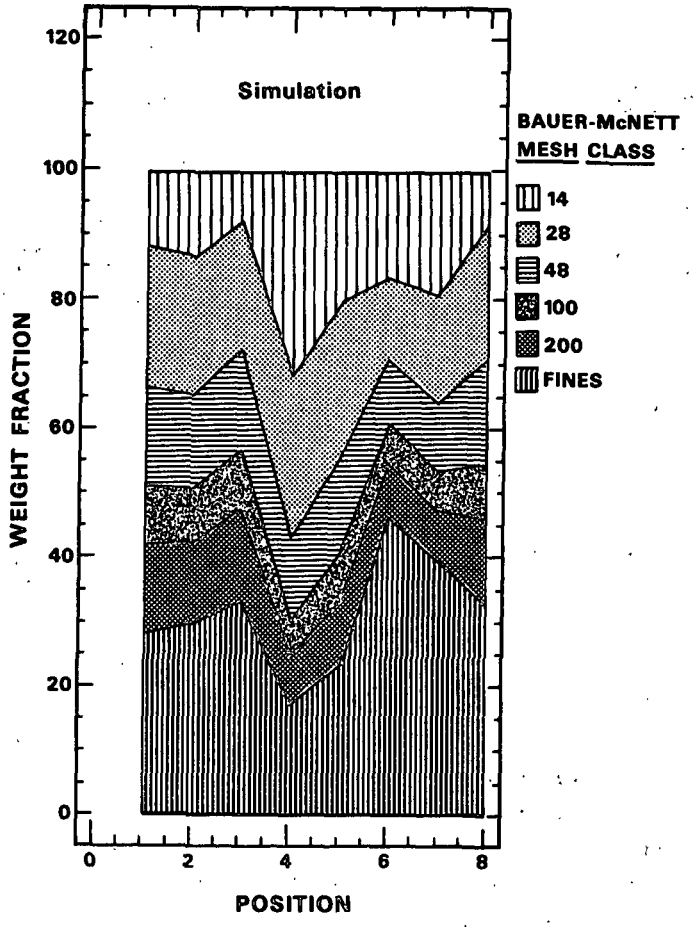

Fig. 3. Predicted fiber length distributions.

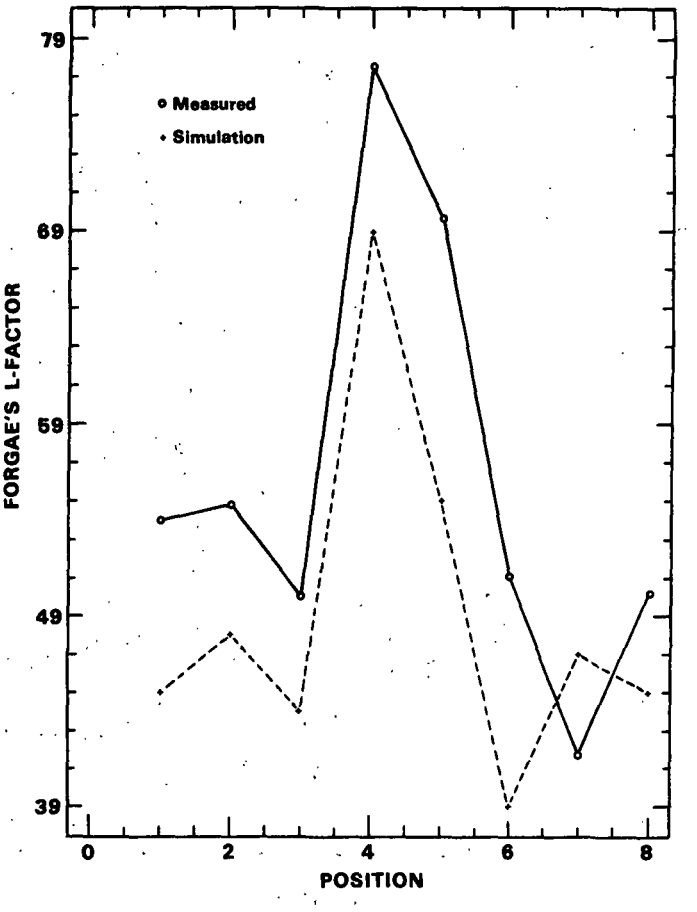

Fig. 5. Forgac's L-factor vs. position.

centrated in the screened rejects and somewhat lower, although not eliminated, from the thickened stock. The shives are all reduced to the smallest width category (Shive 1) during refining. Fines tend to be highest in the reject refiner discharge and the reject cleaner accepts streams, while shives tend to be lowest there.

The trends shown in Figure 5 for Forgac's L-factor, defined as the sum of the 14, 24 and 48 mesh fractions, reflects the fines variations. The error in predicting the distribution in the secondary refiner discharge persists throughout the simulation. This indicates the importance of the adjustment of the refiner parameters in the early part of the process.

The Canadian Standard Freeness profile shown in Figure 6 indicates CSF is predicted quite well, considering the high level of variability inherent in the freeness measurement. The freeness variations are clearly dominated by variations in fines levels. Given this relationship, it is puzzling that the largest error in predicting freeness occurs for stream 5, while the largest error in predicting fines occurs in stream 6 where the freeness prediction is very close.

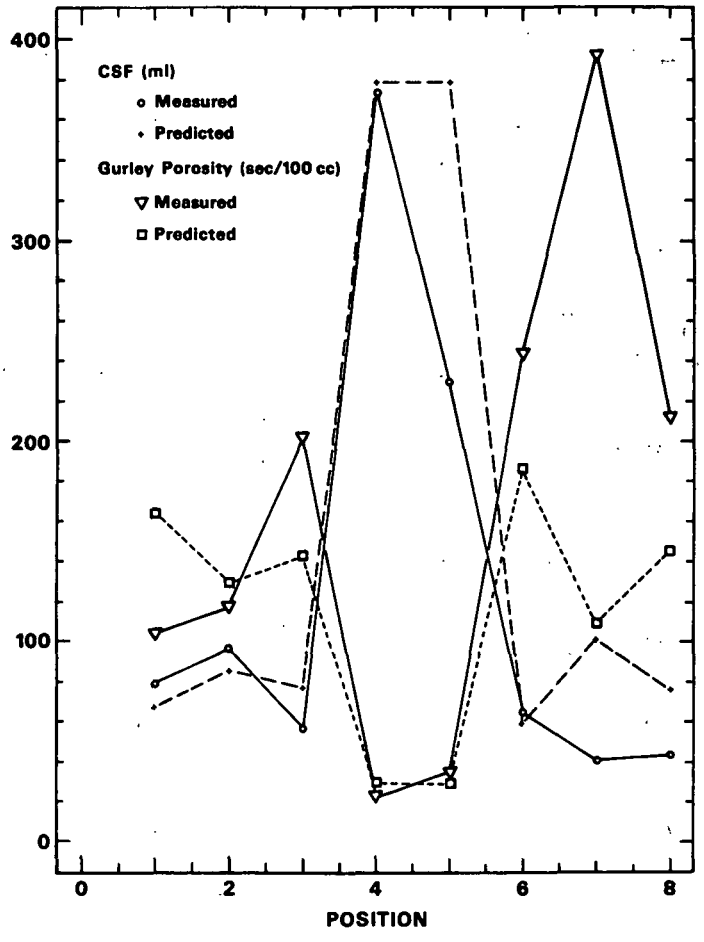

Fig. 6. CSF and Gurley porosity vs. position.

The Gurley porosity was found to be essentially an inverse function of CSF. For this reason the two variables are plotted together in Figure 6. This relationship predicts Gurley porosity quite well. However, it may not hold for a wide variety of pulps.

Figures 7 through 11 show the sheet property variations. It is interesting to note that despite the variety of processing influencing the fibers, many properties of the thickened stock are nearly identical to those of the secondary refiner discharge.

The TAPPI density variation shown in Figure 7 is predicted quite well except for sheets made from the reject cleaner accept stream. Generally the values are within 10%, an acceptable level of error considering the lack of detailed information required for the simulation. The sheet density is lowest for the high freeness reject system pulps and highest for the high fines pulps.

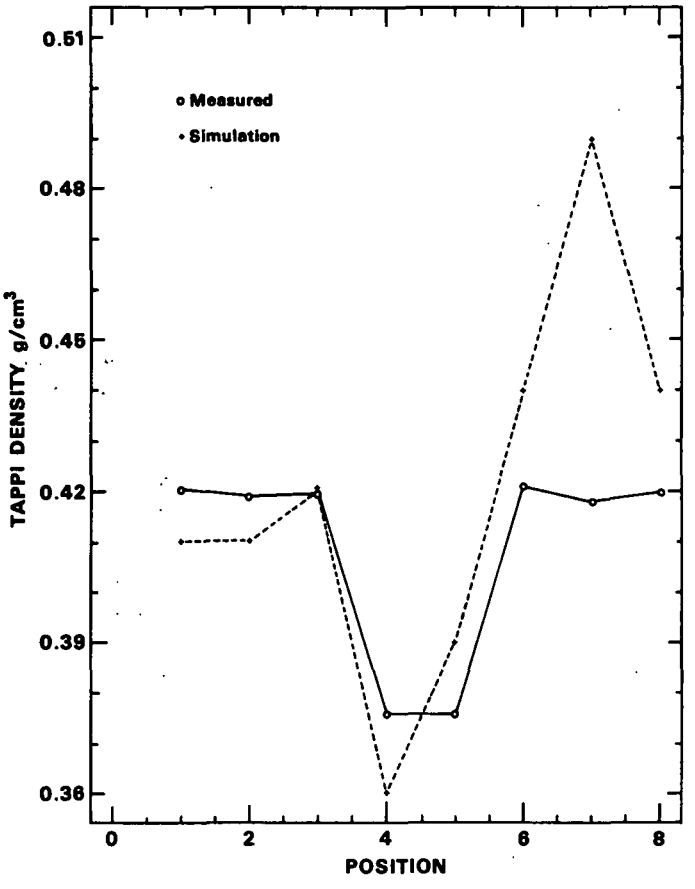

Fig. 7. TAPPI density vs. position.

Breaking length, shown in Figure 8, is also predicted within 10% with the exception of position 5, secondary screen accepts. It is also interesting that the predicted breaking length profile reflects the measured density which does not vary greatly, while the measured breaking length shows a much wider variation through the

system. It is possible the fiber tensile strength (zero span tensile) is influenced by refining and by the fiber length distribution. In the current models, the only influence on fiber tensile or modulus is through density, which is influenced mainly by removal of lignin or hemicellulose in pulping or bleaching and by cell-wall thickness.

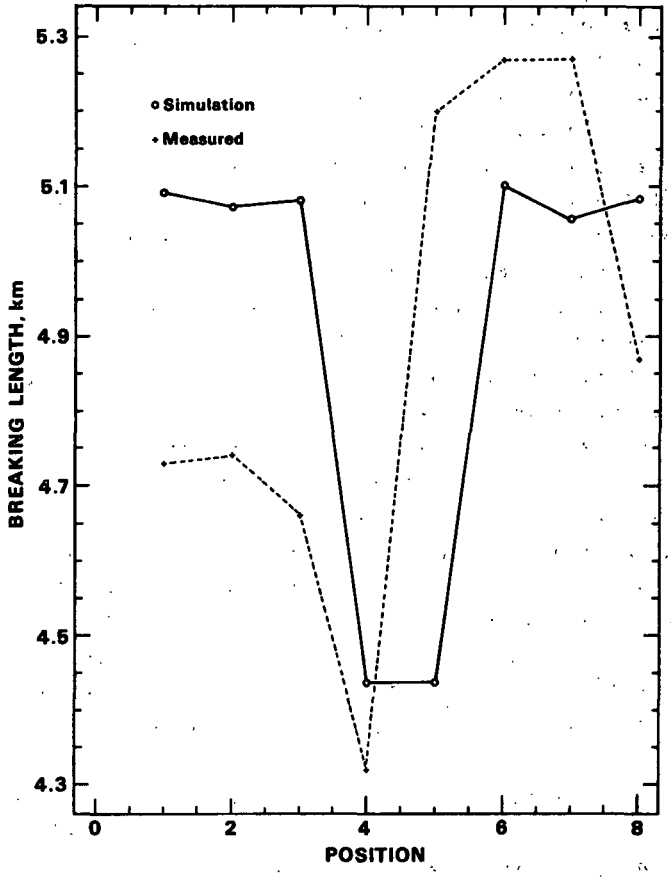

Fig. 8. Breaking length vs. position.

Burst and tear factor profiles in Figure 9 show a very weak trend in burst which fails to reflect the variations in breaking length. The simulation results show a more marked correspondence between burst and breaking length. The measured tear reflects the variations in long fiber content. However, simulation predictions based on the correlative model fail to show a large increase observed in the reject system despite the strong influence of fiber length in this model. Nevertheless, the final tear value is predicted quite accurately.

Scattering coefficient, shown in Figure 10, is also predicted within 10% except for position 6 which probably reflects the error in the fines prediction for that point in the process. Otherwise, these values strongly reflect fines content variations.

Although the details of the elongation at break profile shown in Figure 11 are not well predicted, the general values are within 15 to

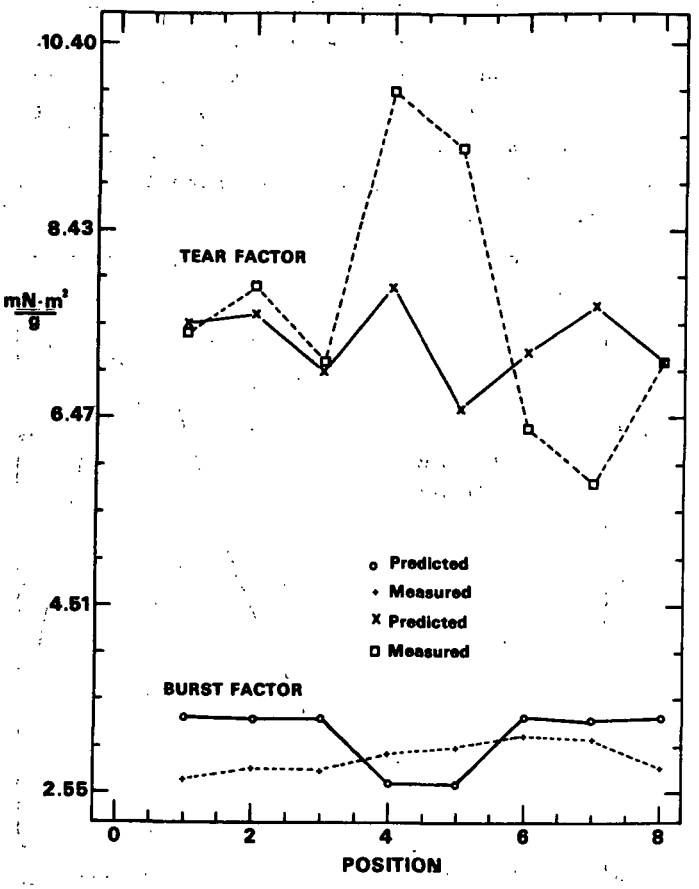

Fig. 9. Burst and tear vs. position.

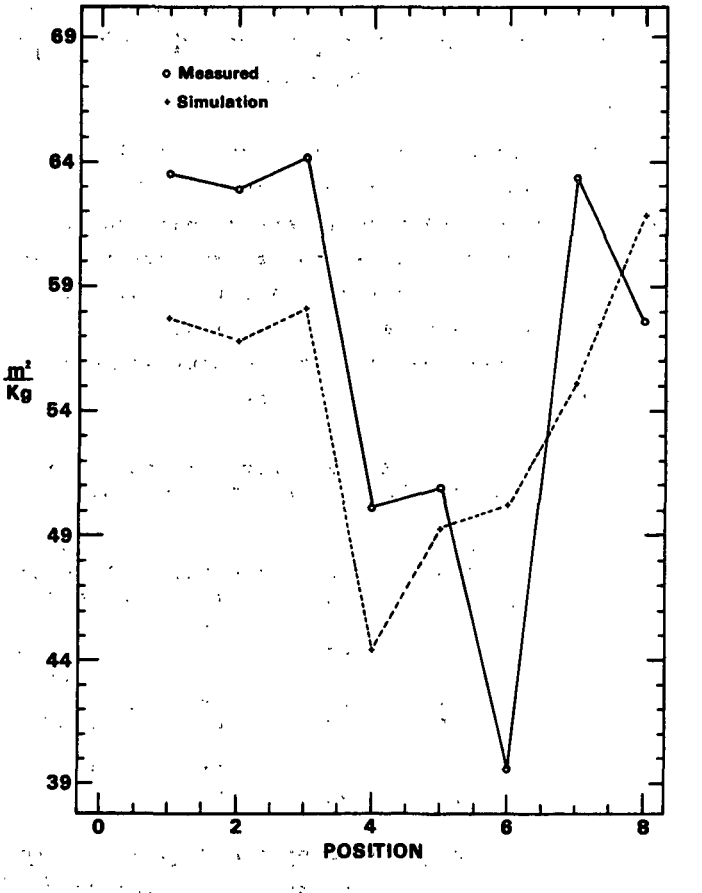

Fig. 10. Scattering coefficient vs. position.

20% except for positions 6 and 7. This is a highly sensitive variable and one that is difficult to predict with high accuracy. However, considering that the model used to predict this was based on chemical pulp measurements and extrapolated to 100% yield, the results are understandable.

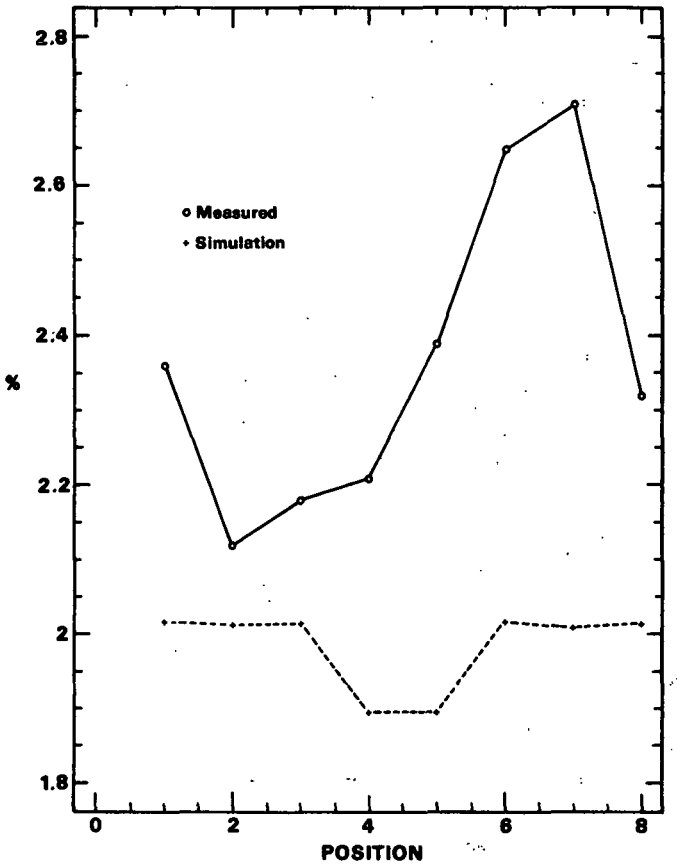

Fig. 11. Elongation at break vs. position.

Drainage time, wet web strength (WWS), brightness and Z-D tensile are summarized in Table V. Drainage time and wet web strength are predicted by the simulation and there are no corresponding data values. Brightness and Z-D tensile are data values with no corresponding simulation predictions at present.

Table V. Predicted Runnability Parameters and Measured Brightness and Z-D Tensile.

Position	Drainage Time s	WWS g	Brightness %	Z-D Tensile kN/m
1	--	66	51	12.6
2	14	67	48	12.3
3	14	71	50	13.3
4	14	57	49	9.5
5	5	60	47	10.4
6	32	81	52	13.1
7	13	73	51	13.5
8	29	72	52	13.3

Simulation of Chemical Pulping and Paper Making

A major expansion of the PAT system to simulate chemical pulping and papermaking is in progress. The new system will be designed to simulate combined high yield and chemical pulping systems as well as species mixtures. A species data base containing chemical and physical property data on various fiber types will be used to initialize PAT streams as well as to determine initial pulp stream compositions.

The new system will determine the effects of pulping and bleaching severity on PAT's such as absorption coefficient, fiber modulus, zero-span tensile, cell-wall-thickness and fiber composition. The refining modules will be modified to account for differences in the response of chemical and high-yield pulps to refining conditions. Mixing and fractionation modules will be modified to account for a larger number of performance attributes.

Papermaking will include the effects on formation of jet-to-wire drag ratio, headbox consistency, and machine speed. Formation will be quantified in terms of a variation of sheet density. A distribution in sheet density will then result in a variation in sheet properties. Wet pressing will include the effects of sheet densification and water removal. Wet straining and fiber orientation will be used to account for changes in sheet anisotropy which will be quantified through the six independent elastic moduli [11,12,13]. Prediction of the six sheet moduli will enable prediction of compressive strength [14].

It also will be necessary to include calendering, additives and coatings. The calender model will include changes in surface structure and optical properties, densification, and reduction in elastic and failure properties due to hardening and brittle failure [15].

CONCLUSIONS

The performance attribute system predicted with reasonable accuracy many handsheet properties and processing conditions throughout a typical TMP mill. Commonly measured handsheet properties are explicable with relatively simple models based on variables whose values are readily attainable. Many strength properties are strongly dependent on sheet density which depends on fiber surface area and fiber-fiber bonding. Other properties such as tear and scattering coefficient depend on fiber morphology and the numbers and types of fibers. Operability factors depend on defects which are related to shive number and size. Much work lies ahead to expand the system to predict a greater variety of end-use performance characteristics for both handsheets and machine-made

papers. The current system provides the foundation which can be easily expanded and modified to add new processing steps and end-use performance characteristics.

ACKNOWLEDGMENTS

The author wishes to acknowledge the support of this work by the member companies of The Institute of Paper Chemistry, both financial and through the advice and data resources provided by their representatives on the Systems Analysis Project Advisory Committee.

REFERENCES

1. PARKER, P. E., Process Simulation as a Decision-making Tool, PIMA, 34-39 (1986).
2. JONES, G. L., Simulating the Development of Pulp and Paper Properties in Mechanical Pulping Systems, Pulp Paper Mag. Can. (July 1988).
3. JONES, G. L., Simulation of Product Quality and Process Performance, Proceedings of the 1987 Eastern Simulation Conference, Orlando, FL, (April 6-9, 1987).
4. YAN, J. F., Kinetic Theory of Mechanical Pulping, Tappi J., 58(7):156-158 (1976).
5. STRAND, B. D. and L. L. EDWARDS, Optimal Design, Operation, and Control of Mechanical Pulping Systems, Tappi J., 67(12):72-75 (1984).
6. STATIONWALA, M. I., D. ATACK, J. R. WOOD, D. J. WILL, and A. KARNIS, International Mechanical Pulping Conference, Toronto, Canada (1979).
7. VENKATESH, V., A Systems Engineering Approach to Effluent Control, Pulp Characterization and Process Design in Mechanical Pulp Mills, Ph.D. Dissertation, U. of Idaho (1976).
8. MOLDENIUS, S., Kinetic Models for Hydrogen Peroxide Bleaching of Mechanical Pulps, J. Wood Chem. Technol. 2(4):447-71 (1982).
9. ALEXANDER, S. D., R. MARTON, and S. D. McGOVERN, Tappi J. 51(6):277 (1968).
10. ULLMAN, U., O. BILLING, and A. JONSSON, Fibre Classification as a Method of Characterizing Pulp", Pulp Paper Mag. Can., Technical Paper T331, 69-83 (Sept. 1968).
11. PAGE, D. H. and R. S. SETH, The Elastic Modulus of Paper, II. The Importance of Fiber Modulus, Bonding and Fiber Length, Tappi J. 63(6):113 (1980a).
12. BAUM, G. A., D. G. BRENNAN, and C. C. HABEGER, Orthotropic Elastic Constants of Paper, Tappi J. 64(8):97 (1981).
13. FLEISCHMAN, E. H., G. A. BAUM, and C. C. HABEGER, A Study of the Elastic and Dielectric Anistropy of Paper, Tappi J., 115-118 (Oct. 1982).
14. HABEGER, C. C. and W. J. WHITSITT, A Mathematical Model of Compressive Strength in Paperboard, Fiber Science & Technology, 19:215-239 (1983).
15. CHARLES, L. A. and J. F. WATERHOUSE, The Effect of Supercalendering on the Strength Properties of Paper, J. of Pulp and Paper Science, 14(3), J59-65 (1988).